Appl Phys B (2010) 100: 93–100
DOI 10.1007/s00340-010-4065-z

Applied Physics B
Lasers and Optics

Toward superlensing with metal–dielectric composites and multilayers

R.B. Nielsen · M.D. Thoreson · W. Chen · A. Kristensen · J.M. Hvam · V.M. Shalaev · A. Boltasseva

Received: 24 April 2010 / Published online: 29 May 2010

Abstract We report on the fabrication of two types of adjustable, near-field superlens designs: metal–dielectric composites and metal–dielectric multilayer films. We fabricated a variety of films with different materials, thicknesses and compositions. These samples were characterized physically and optically to determine their film composition, quality, and optical responses. Our results on metal–dielectric composites indicate that although the real part of the effective permittivity generally follows effective medium theory predictions, the imaginary part does not and substantially higher losses are observed. Going forward, it appears that multilayer metal–dielectric designs are more suitable for sub-diffraction imaging applications because they could provide both tunability and low loss.

R.B. Nielsen · J.M. Hvam · A. Boltasseva
DTU Fotonik – Department of Photonics Engineering, Technical University of Denmark, Lyngby, Denmark

M.D. Thoreson · A. Boltasseva
Erlangen Graduate School in Advanced Optical Technologies (SAOT), Friedrich-Alexander-Universität Erlangen-Nürnberg, 91052 Erlangen, Germany

M.D. Thoreson · W. Chen · V.M. Shalaev (✉) · A. Boltasseva
School of Electrical and Computer Engineering and Birck Nanotechnology Center, Purdue University, West Lafayette, IN 47907, USA
e-mail: shalaev@purdue.edu

A. Kristensen
DTU Nanotech – Department of Micro- and Nanotechnology, Technical University of Denmark, 2800 Kgs., Lyngby, Denmark

1 Introduction

For a long time it was thought to be fundamentally impossible to focus light below the diffraction limit, a paradigm that changed in the year 2000 with the proposal of a sub-diffraction superlens by Pendry [1], which was based on the 1968 paper on negative-index materials by Veselago [2]. Included in Pendry's proposal was a simplified, near-field superlens design that requires only a negative permittivity, rather than simultaneously negative permittivity and permeability. Near-field superlensing was experimentally demonstrated in 2005 by Fang and co-workers [3] and nearly simultaneously by Melville and Blaikie [4], followed by others [5]. However, the practical applications of near-field superlenses are still quite limited, since superlensing requires that the matching condition $\varepsilon_{\text{metal}} = -\varepsilon_{\text{dielectric}}$ is met [1]. For dispersive materials this limits operation to a single wavelength for each material system. For the most commonly used silver–polymer combination, the matching condition is met at a wavelength of around 365 nm [2–4]. Thus far, no demonstrations have been made of superlensing in the visible or near-infrared regions that have the most promising applications. Several solutions have been proposed to bring superlensing to these spectral ranges, including the use of metal–dielectric composites (MDCs) [6–9] and multilayer lens structures [10–15].

Multilayer superlens designs have received considerable attention due to their enhanced resolution as compared to a single-layer superlens and also due to their relative robustness to losses. Functioning at the plasmon resonance of the individual layers leads to subwavelength resolution, but the large impedance mismatch renders the system impractical [16]. The alternating layers of metal and dielectric can also have subwavelength resolution away from the individual-layer plasmon resonances, which leads to tunability and tolerance to losses along with the possibility of

impedance matching [17]. The analysis in this regime proceeds by an effective medium theory and leads to a condition determined by impedance matching and the isofrequency curve of bulk propagating waves within the medium rather than the individual-layer plasmon resonances. The design of the multilayer superlens involves many subtle issues with regard to the total number of layers, the choice of the initial and final layers, individual layer thicknesses, total lens thickness and also the object itself [18]. Due to the large reflections that are inevitable when using a metal-based structure, the resolution often depends on the coupling between the object to be imaged and the superlens, hence the design has to be modified and optimized accordingly [19].

MDCs are materials that consist of a random mixture of metallic and dielectric particles. Through the use of either MDCs or multiple layers, it is possible to tune the superlens operational wavelength for a particular application simply by altering the volume ratio between the metal and dielectric components in the composite. By "tunable" here we mean that the operational wavelength of the superlens can be selected prior to fabrication. If such a tunable superlens can be achieved, it opens up many promising applications based on the spatial translation (transfer) of highly localized, enhanced electromagnetic fields [20–27] created e.g. by nanoantennas [28–31] to the other side of a superlens [32], with possible applications in surface-enhanced Raman spectroscopy (SERS) [33] or enhanced fluorescence microscopy [34].

In this paper, we present the results of our studies on the fabrication and characterization of various MDC films and multilayer structures. Composite films were fabricated using two different material combinations and with a variety of compositions. These films were characterized structurally by atomic force microscopy (AFM) and scanning electron microscopy (SEM) imaging. In addition, they were optically characterized by spectroscopic ellipsometry and far-field transmission and reflection measurements. The effective dielectric permittivity of each sample was found by fitting to the experimental results. Furthermore, we determined the exact composition for many of the films through the use of energy dispersive x-ray spectroscopy (EDX). Using the composition information, we then compared our results to those predicted by an effective medium theory. We also present results on the fabrication of multilayer structures using a combination of materials, with the characterization of these samples involving the same methods as we used for the MDC films. Finally, we investigated the use of wetting layers in order to improve the quality of multilayer structures. The overall goal of our project is to achieve tunable, or adjustable, optical material properties and to exploit these properties for superlensing at frequencies in the visible and near-infrared wavelength ranges.

2 Methods of tuning the superlens operational frequency

As mentioned earlier, the superlensing effect depends on matching the permittivities of the superlens material and its surrounding host medium, which makes the proper choice of materials a critical factor in designing a superlens. Given this limitation, there are three ways of designing a superlens with a particular operational wavelength. The most basic method is choosing a metal–host combination that directly achieves the matching condition. Some examples of this situation can be seen in Fig. 1, where we show the real part of the permittivity for a number of dielectric materials as well as the permittivity of silver with the opposite sign. The points of intersection between the silver and each dielectric indicate wavelengths at which the matching condition is satisfied. This method can be problematic, however, since silver is the only metal with low enough loss in the visible range, and suitable host materials exist only for a few operational wavelengths. Furthermore, each time the operational wavelength is changed, a new fabrication process will have to be developed, which can be quite impractical.

The difficulty and lack of adaptability in using differing host materials for each new application brings us to the other two methods that are the focus of this paper: MDCs and multilayer structures. A schematic of these schemes can be seen in Fig. 2.

A number of effective medium theories (EMTs) have been developed to describe various types of composites [35–39]. As the basis for this study, we chose Bruggeman's EMT [39], which predicts that the following relation exists

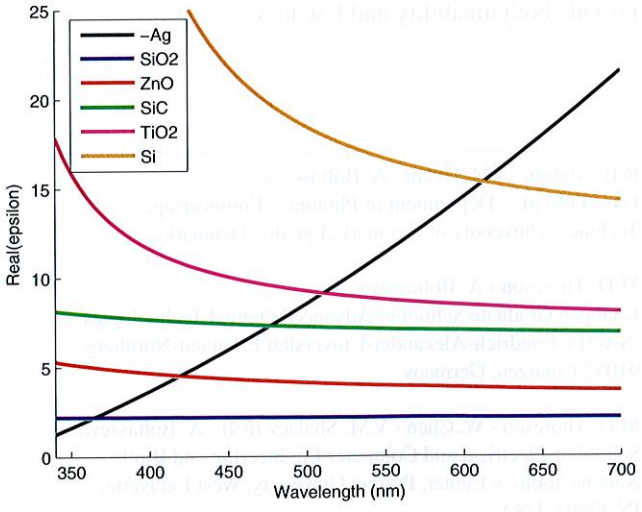

Fig. 1 Resonance wavelengths (intersection points) for silver in combination with several dielectric materials within the visible wavelength range. All permittivities are for bulk materials. The negative of the Ag real permittivity is shown for easy identification of the resonance intersection points

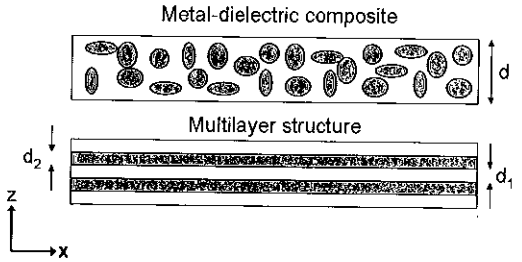

Fig. 2 Schematic of a random metal–dielectric composite film (*top*) and a multilayer system (*bottom*). Each scheme provides a method of adjusting the operational wavelength of a superlens

for the permittivity of a two-component mixture of a metal and a dielectric:

$$p\frac{\varepsilon_m - \varepsilon_e}{\varepsilon_m + (d-1)\varepsilon_e} + (1-p)\frac{\varepsilon_d - \varepsilon_e}{\varepsilon_d + (d-1)\varepsilon_e} = 0 \qquad (2.1)$$

where subscript m refers to the metal, d to the dielectric, and e to the effective medium. The dimensionality of the system is given by the factor d, The filling factor p is defined as

$$p = \frac{V_m}{V_{\text{total}}}. \qquad (2.2)$$

Hence, Bruggeman's EMT predicts that the effective optical properties of the MDC can be controlled simply by varying the filling factor of one of the materials in order to achieve the desired permittivity for a particular application. Combined with the superlens matching condition, this means that the operational wavelength can be tuned by altering the filling factor while keeping the same material combination and host, which greatly simplifies the fabrication process.

For lamellar, multilayered systems such as that shown in the bottom panel of Fig. 2, the situation is slightly more complex. These systems can be considered to be uniaxial crystals that exhibit a flat hyperbolic dispersion relation [10, 11]. Multilayered systems have been extensively studied theoretically, and their lensing and optical properties have been discussed by a number of authors [11–15]. A metal–dielectric multilayered system with subwavelength layer thicknesses exhibits an anisotropic permittivity characterized by the flat hyperbolic dispersion function [11]

$$\varepsilon_x = \varepsilon_y = \frac{\varepsilon_d d_1 + \varepsilon_m d_2}{d_1 + d_2}, \varepsilon_z = \left(\frac{\varepsilon_d^{-1} d_1 + \varepsilon_m^{-1} d_2}{d_1 + d_2}\right)^{-1}, \qquad (2.3)$$

where the coordinate directions and materials are identified in Fig. 2. In superlensing applications, we are interested in obtaining a system with a parallel permittivity of unity for impedance matching ($\varepsilon_x = \varepsilon_y = 1$) and an infinite perpendicular permittivity ($\varepsilon_z \to \infty$). This is known as the canalization regime [11]. In practice, however, due to losses and material limitations, both conditions cannot be fulfilled simultaneously.

Unlike the matching condition for single films, this does not limit operation to a single wavelength for a given material combination, but rather allows the operational wavelength to be tuned simply by altering the relative thicknesses of the metal and dielectric layers, thus allowing tunability similar to that found for superlenses based on MDC films.

Another condition for optimizing the performance is the size of the device [17]. The spatial frequency information of the object is carried by bulk propagating waves within the multilayer structure to the output interface. The transfer function characterizes the propagation of waves and also the final spatial spectrum available for image reconstruction. Selecting an appropriate thickness which leads to a Fabry–Perot resonance condition helps to provide a flat transfer function for the various spatial frequencies. The image at the output interface is then a faithful reconstruction of the object with subwavelength resolution. This resonance condition is not tolerant to deviations, and the stringent restriction is difficult to achieve in the optical frequency domain [40]. Image distortions arise due to a transfer function which is not flat and hence numerical optimization for the size of the device is the best route to design the multilayer structure.

3 Metal–dielectric composites

In our fabrication of MDC films, we employed two different methods, one for each of the dielectrics used. Silver was used as the metal in both cases, since it has the lowest loss in the visible range. The dielectrics we used were silicon dioxide (SiO_2) and zinc oxide (ZnO); these were chosen based on their permittivities and fabrication compatibilities.

3.1 Ag/ZnO composites

The Ag/ZnO MDC films described in this section were fabricated in a DC sputtering system. Since the deposition chamber used had six individually powered sputtering guns, we were able to perform simultaneous sputtering of both the silver and zinc oxide materials. This approach creates a uniform, isotropic film. During sputtering, no substrate bias or heating was used, and the pressure was kept constant at 5 millitorr. In order to prevent oxidization of the silver, no oxygen flow was used, so the only gas present in the chamber was the argon plasma. The use of simultaneous sputtering meant that the film composition could be controlled by varying the sputtering power for the individual guns, and thus changing the deposition rate for each material.

Two different types of Ag/ZnO samples were created for our studies. One type consisted of thick films (>100 nm) on silicon substrates, while the other type consisted of thinner, 35-nm films, deposited on fused silica substrates. The thick

films were made for optical characterization via ellipsometry, which simplified the fitting procedures of the ellipsometry data because with such a thick film we could assume the presence of only a single interface, and thus we could determine the bulk optical properties of the film with relative ease. Furthermore, the larger thickness helped increase the signal-to-noise ratio in our subsequent EDX characterization, and thus we were able to improve the accuracy with which the composition of the MDC film could be determined. The thin films on fused silica substrates were used for optical characterization via far-field transmission and reflection measurements and also for easy comparisons of our AFM roughness results to previous papers [2–4]. AFM characterizations of the Ag/ZnO MDC films show that the roughness remains below 1 nm RMS (root mean square) for filling factors between 0.7 and 0.9. The 1-nm RMS roughness value is generally considered a good benchmark for high-quality metal films and is very similar to what has been used successfully to demonstrate near-field superlensing in the past [2–4]. The mean grain size in the films was found to be very uniform and around 20 nm. For filling factors either above or below this range, the roughness values increase. It is important to note that the roughness is also significantly higher for a filling factor of 1, corresponding to a pure silver film. This can be explained by considering the growth mechanism of silver films on a quartz substrate. Silver has a high surface energy on fused silica, which leads to island formation rather than wetting. These individual islands grow in size as more metal is deposited until they merge together to form a complete layer. Such a growth mode leads to large grain sizes, and thus the film exhibits high surface roughness. However, silver has a lower surface energy on ZnO, and thus the simultaneous deposition of this material tends to break up the island growth and leads to the formation of many smaller grains rather than a few large grains. This can be considered a kind of built-in wetting layer.

In an attempt to further reduce the roughness, experiments were carried out using a thin germanium layer on the fused silica substrate, since this has been proven very effective in reducing roughness for pure silver [12] and silver/silica multilayers [41]. However, we did not observe this wetting effect, or a lower roughness, for Ag/ZnO composites. The roughness was found to be the same both with and without the presence of a germanium layer. Thus, the roughness in Ag/ZnO composites appears to be intrinsic to the growth of the composite itself, rather than being dominated by surface (substrate) interactions as is typically the case when depositing thin metal films.

The determination of the filling factor by EDX measurements was performed using an FEI Nova 600 NanoSEM and Oxford INCA software, with the acceleration voltage kept constant at 10 kV. Since EDX provides data on the atomic composition of films, but EMT requires volume composition, some calculations were needed to convert the EDX data into a usable form. These calculations were based on the different lattice parameters of Ag and ZnO, using bulk parameters. The calculations were based on the amount of Ag and Zn present, since oxygen might be present in several different forms, including SiO_2 on the surface of the substrate and Ag_2O in the composite after exposure to air, and thus would not provide a direct indication of the amount of ZnO present.

With the EDX measurements, we were able to accurately determine the filling factor of the constituent materials, which proved to be very constant across the entire sample, with a variation of no more than 1–2% for different measurement areas. By looking at the EDX results, and varying the sputtering powers for each gun accordingly, we were able to achieve values ranging from 0.55 to 0.88, which covers nicely our region of interest.

The ellipsometer was mounted directly on the deposition chamber, in such a way that measurements could be performed in vacuum conditions. This is critical because the films degrade in air when no protective layer is present, which results in a change of their optical properties. The downside of having an in situ ellipsometer was that it had a fixed position, so the angle could not be changed between measurements.

Using the ellipsometry measurements we were able to accurately fit the optical properties of the fabricated MDC films. The results, as shown in Fig. 3, confirm that it is possible to tune the real part of the permittivity over a wide range, as it was predicted by Bruggeman's theory. This shows that using MDCs it is possible to achieve virtually any combination of permittivity and wavelength one desires, and opens up the possibility of creating a superlens with an operational frequency anywhere in the visible wavelength range. For the loss, the situation is different, and all the fabricated films have losses far higher than pure silver. The general trend is that a lower filling factor is associated with higher loss.

3.2 Ag/SiO_2 composites

Ag/SiO_2 MDC films of various thicknesses and compositions were deposited on glass substrates (microscope slides) at room temperature. For this purpose we used both an RF/DC sputtering system and an E-beam evaporations system. Shortly before the evaporation process, the glass substrates were submerged in a piranha (H_2O:$2H_2SO_4$) bath for 20 minutes and were then washed with water. The substrates were then rinsed multiple times with acetone and isopropanol and finally dried with gaseous nitrogen. The initial pressure in the sputtering chamber was approximately 10^{-6} torr. Silver and silicon dioxide layers were deposited in very thin, alternating layers during the same evaporation

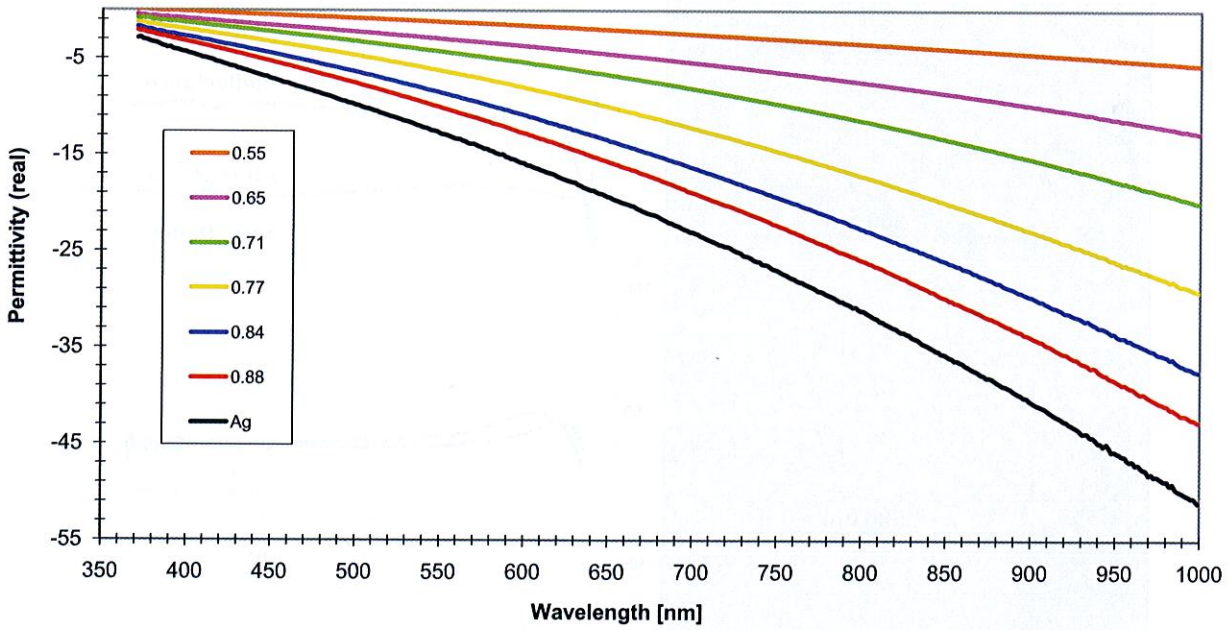

Fig. 3 Fitted real part of the permittivity of Ag/ZnO composite films with varying filling factors. By adjusting the metal filling factor, it is possible to tune the permittivity over a wide range of values

process, and the substrates were rotated at a few revolutions per minute during the deposition process to ensure uniform material coverage. Due to the extremely small amount of material deposited in each sublayer, the overall film is a composite structure resembling a random mixture of metal and dielectric.

The fabricated films were characterized using AFM, far-field spectral measurements and spectroscopic ellipsometry. The AFM measurements were performed using a Veeco NanoMan system AFM in tapping mode with standard silicon tips, a scan size of 2×2 μm, and a scan rate of 1 Hz. The spectroscopic ellipsometry measurements of the films were obtained using a J.A. Wollam V-VASE system in the 0.3–1.7 μm range and at several angles of incidence. The far-field transmittance spectra of the films at normal incidence were measured with a Lambda 950 spectrophotometer (Perkin Elmer) in the 0.3–2.5 μm wavelength range. The reflectance spectra of the films were measured at 8° incidence in the 0.3–2.5 μm wavelength range using a 150-mm integrating sphere accessory and the spectrophotometer. The wavelength step size for both transmittance and reflectance measurements was set at 5 nm. The experimental curve was obtained by performing a point-by-point fit of the ellipsometry data for the sample.

We fabricated several composite films with varying layer numbers and thicknesses in order to investigate whether EMT would correctly predict the optical responses of the films. Three such films are shown in Fig. 4, where representative SEM images are shown along with measured far-field spectra for each sample. The total film thicknesses and metal filling factors were kept constant at 47 nm and 65% for the three films shown in the figure, and hence EMT predicts that the films should exhibit the same optical responses. However, the measured far-field spectral responses are clearly different for the three films, and the SEM images show differing structures of the films as well. Hence, this is a sign that the EMT is not completely accurate for these composite films.

3.3 Comparison with effective medium theory

When comparing our fitted values of the permittivity with those found from EMT, it is clear that a more comprehensive theory is needed. The real part of the permittivity is reasonably close to that expected from theory, but the loss is far higher and the absorption band predicted by EMT is not evident. An example of this can be seen in Fig. 5, which shows data for two different MDC films, one based on Ag/ZnO and one based on Ag/SiO_2. The behavior for the two films is seen to be very similar quantitatively, which indicates that the deviation from EMT is not unique, and indeed all fabricated films deviated substantially from EMT in the imaginary part of permittivity.

The cause for this deviation from EMT can be ascribed to a number of things, though they all share a common theme: EMT is too simplified to accurately predict the behavior of these complex structures. Thus a more comprehensive theory is needed, which takes into account factors like particle size and shape, interparticle resonances and film uniformity.

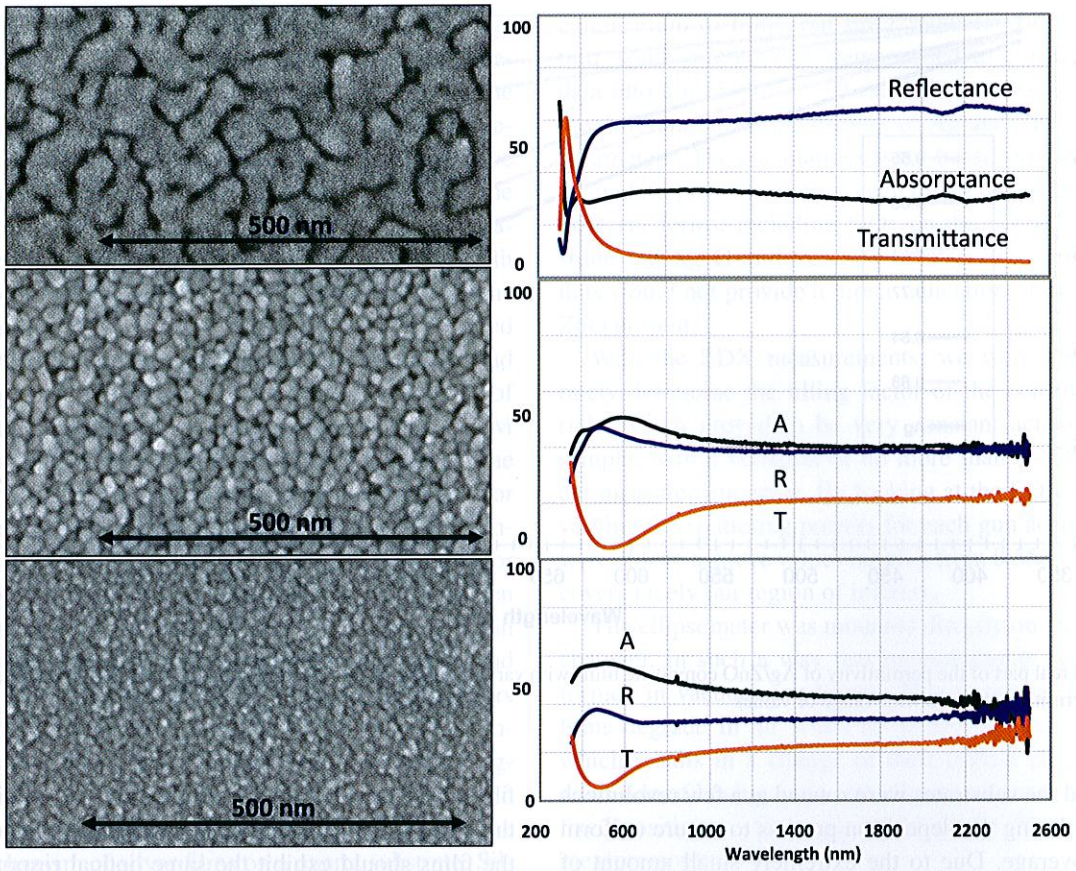

Fig. 4 SEM images of Ag/SiO_2 composite near-field superlens prototypes and their associated far-field spectral measurements. For all films, the thickness is 47 nm and the silver volume ratio is 65%. EMT predicts that these films should show the same effective behavior

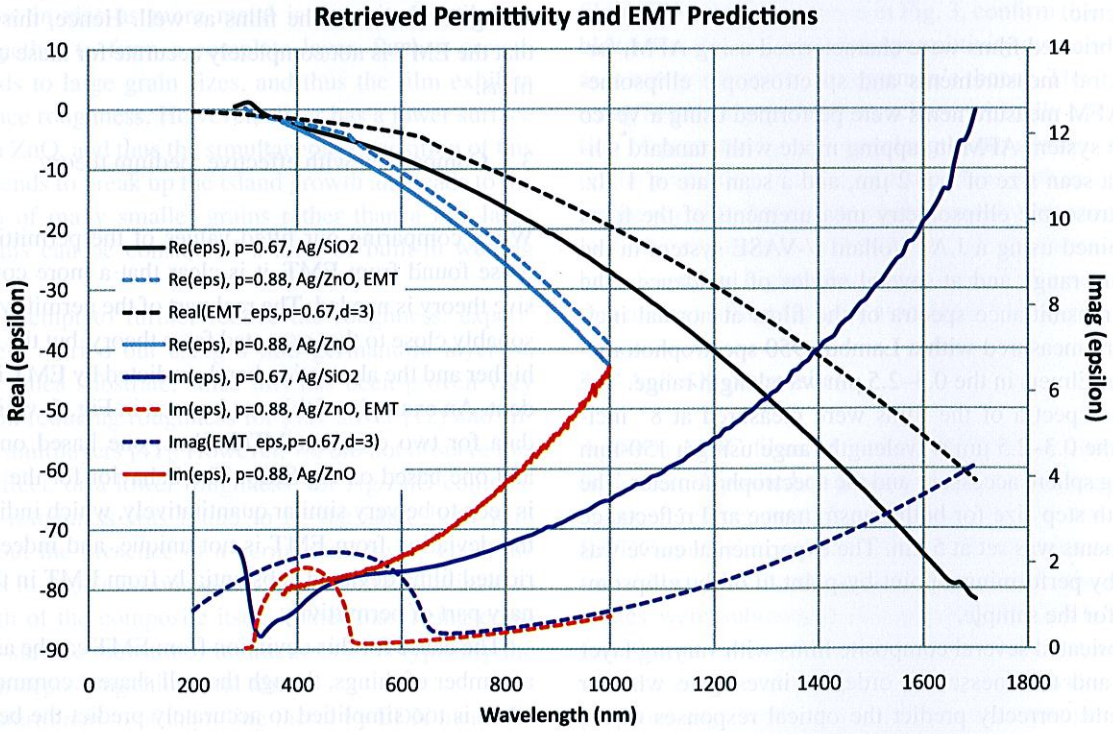

Fig. 5 Real and imaginary parts of permittivity for simulated and experimental films. Experimental data are shown in *solid lines*, while EMT-based simulations are shown in *dashed lines*. In particular, the imaginary values of permittivity for the experimental films are far higher than their simulated counterparts. Two experimental films are shown: one is a 67% Ag/SiO_2, the other is an 88% Ag/ZnO film

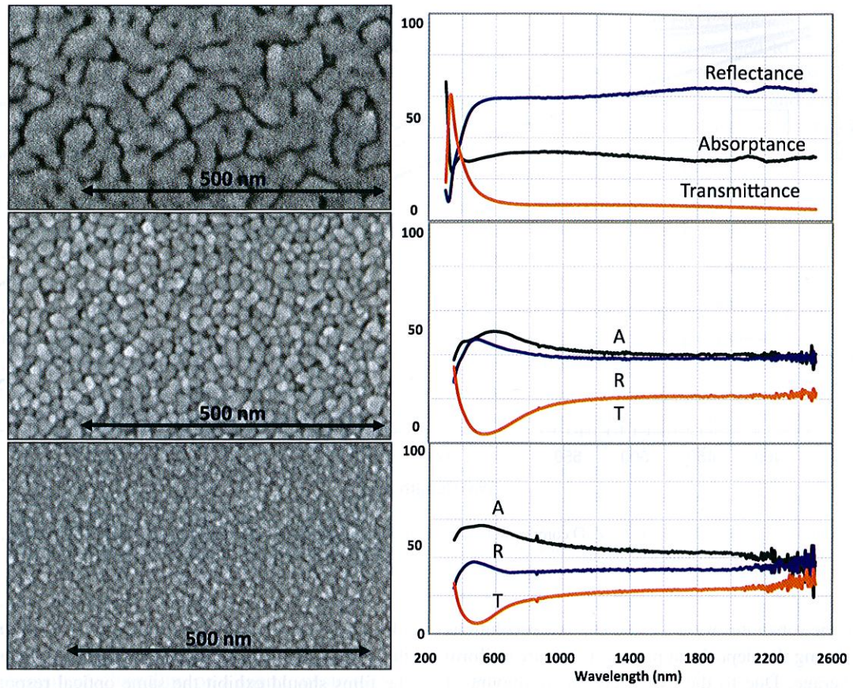

Fig. 4 SEM images of Ag/SiO_2 composite near-field superlens prototypes and their associated far-field spectral measurements. For all films, the thickness is 47 nm and the silver volume ratio is 65%. EMT predicts that these films should show the same effective behavior

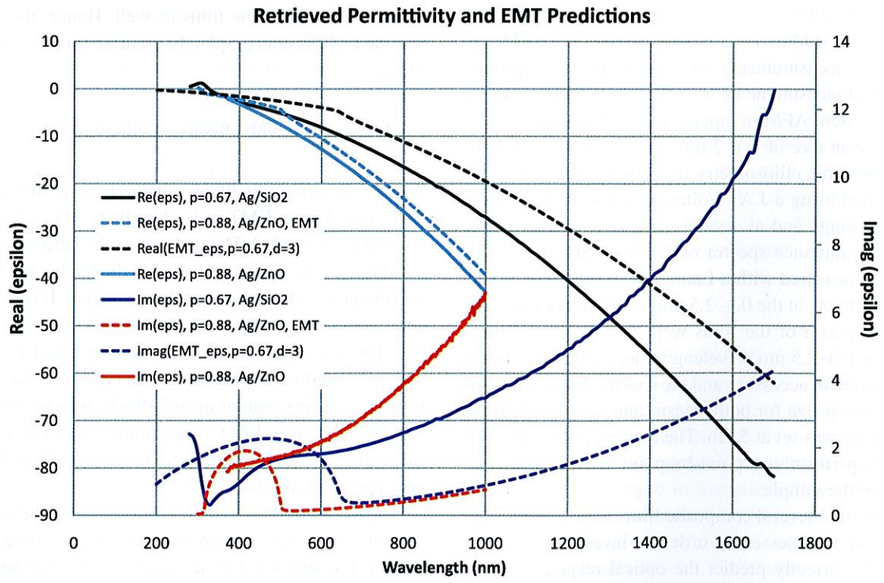

Fig. 5 Real and imaginary parts of permittivity for simulated and experimental films. Experimental data are shown in *solid lines*, while EMT-based simulations are shown in *dashed lines*. In particular, the imaginary values of permittivity for the experimental films are far higher than their simulated counterparts. Two experimental films are shown: one is a 67% Ag/SiO_2, the other is an 88% Ag/ZnO film

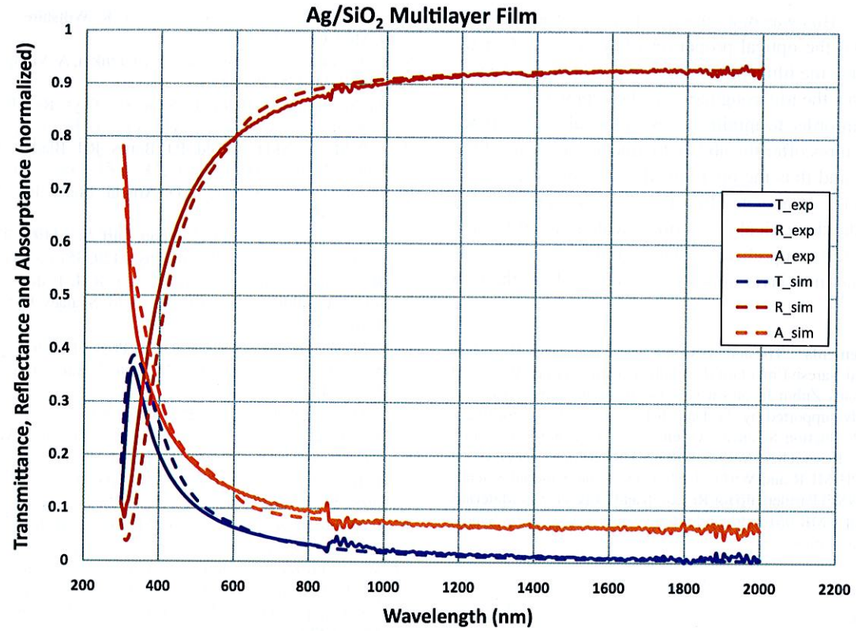

Fig. 6 Measured and simulated far-field spectral responses for (10 nm Ag/1 nm Ge/10 nm $SiO_2)_3$ lamellar composite film. The *solid lines* represent the experimental results, while the *dashed lines* represent the simulation results. (Adapted from [41])

4 Multilayer structures

In addition to composites, we started to study lamellar, multilayer metal–dielectric systems, as shown schematically in Fig. 2 (bottom). Previous work has shown that the "devil is in the details" when it comes to the fabrication of a useful multilayered superlens design. In particular, the interfaces between the metal and dielectric layers must be sufficiently smooth in order to reduce the scattering loss in the system. This then imposes a roughness restriction on the interface. A roughness of about 1 nm RMS or lower is necessary for good performance in bulk silver superlensing [3], and we use the same metric in our work as a goal for interface roughness. The metal sublayer thickness is another critical parameter for multilayer superlenses. If the total thickness is kept fixed, a superlens with a smaller metal sublayer thickness provides better superlensing performance [15]. Our previous work [41] has shown that it is possible to obtain a low final roughness and small metal sublayer thicknesses for multilayered silver and silica films by including a very thin Ge wetting layer with each metal/dielectric layer pair. The final roughness of such multilayer films was found to be around 0.3–0.7 nm. Those results also indicate that a continuous silver sublayer was achievable for thicknesses of 5.5 nm or larger when a Ge wetting layer was used. Such a design shows reliable, predictable optical properties, as seen in Fig. 6. In Ag/ZnO multilayer systems, we have found that the Ge wetting layer is not necessary and a low final roughness is achieved only through careful fabrication.

In addition to the Ag/SiO_2 multilayer structures, some Ag/ZnO multilayer samples were also fabricated. This was done in order to investigate if the roughness could be kept low enough without having to use a Ge wetting layer and to provide another option in designing a frequency tunable superlens. The Ag/ZnO stacks all contained 40 nm of silver, and 30–40 nm of ZnO, which was divided into 3–9 layers. All these multilayer structures were made with ZnO capping layers on top and bottom, so as to maintain a symmetric environment. The resulting roughness was found to be 0.9–1.2 nm RMS, depending on the number of layers. Far-field optical characterization was carried out on these films, which displayed optical responses very similar to the Ag/SiO_2 film shown in Fig. 6.

5 Conclusion

We have demonstrated the fabrication of two types of material systems suitable for the creation of a tunable superlens in the forms of metal–dielectric composite films and multilayer stacks. We fabricated and characterized a large variety of both types of structures, varying both materials and

composition. This was done in order to investigate both the structural and the optical properties of such films. Our results show that the film composition can be controlled accurately, and that the film roughness can be kept within acceptable limits in order to minimize loss. Optically, both types of film structures offer the ability to tune the real part of the permittivity and thus the operational wavelength of the superlens. For the composite films, however, the optical losses far exceed the theoretical predictions, which underlines the need for a more comprehensive theory and leaves us to conclude that the multilayer approach currently offers the best solution.

Acknowledgements The authors would like to thank Paul West, Gururaj Naik, and Naresh Emani for their help at a crucial time. We would also like to thank Zubin Jacob for very useful discussions. This work was financially supported by the Danish Research Council for Technology and Production Sciences (Grant No. 274-07-0057), the 2009 SAOT Young Researcher Award, ARO-MURI awards under Grant Nos. 50342-PH-MUR and W911NF-09-1-0539, the National Science Foundation (NSF) Partnership for Research and Education in Materials (PREM) Grant DMR 0611430, and a fellowship sponsored by Sandia National Laboratories.

References

1. J.B. Pendry, Phys. Rev. Lett. **85**, 3866 (2000)
2. V.G. Veselago, Sov. Phys. Usp. **10**, 509 (1968)
3. N. Fang, H. Lee, C. Sun, X. Zhang, Science **308**, 534 (2005)
4. D.O.S. Melville, R.J. Blaikie, Opt. Express **13**, 2127 (2005)
5. C. Jeppesen, R.B. Nielsen, A. Boltasseva, S. Xiao, N.A. Mortensen, A. Kristensen, Opt. Express **17**, 22543 (2009)
6. W. Cai, D.A. Genov, V.M. Shalaev, Phys. Rev. B **72**, 193101 (2005)
7. A.V. Kildishev, W. Cai, U.K. Chettiar, H.-K. Yuan, A.K. Sarychev, V.P. Drachev, V.M. Shalaev, J. Opt. Soc. Am. B **23**, 423 (2006)
8. L. Shi, L. Gao, S. He, B. Li, Phys. Rev. B **76**, 045116 (2007)
9. L. Shi, L. Gao, S. He, *Proc. Int. Symp. Biophot. Nanophot. Metamat.* (2006), pp. 463–466
10. Z. Jacob, L.V. Alekseyev, E. Narimanov, Opt. Express **14**, 8247 (2006)
11. P.A. Belov, Y. Hao, Phys. Rev. B **73**, 113110 (2006)
12. P. Chaturvedi, N.X. Fang, Mater. Res. Soc. Symp. Proc. **919**, 0919-J04-07 (2006)
13. B. Wood, J.B. Pendry, D.P. Tsai, Phys. Rev. B **74**, 115116 (2006)
14. E. Shamonina, V.A. Kalinin, K.H. Ringhofer, L. Solymar, Electron. Lett. **37**, 1243 (2001)
15. S.A. Ramakrishna, J.B. Pendry, M.C.K. Wiltshire, W.J. Stewart, J. Mod. Opt. **50**, 1419 (2003)
16. A. Dorofeenko, A. Lisyansky, A. Merzlikin, A. Vinogradov, Phys. Rev. B **73**, 235126 (2006)
17. M. Silveirinha, P. Belov, C. Simovski, Phys. Rev. B **75**, 035108 (2007)
18. C.P. Moore, M.D. Arnold, P.J. Bones, R.J. Blaikie, J. Opt. Soc. Am. A **25**, 911 (2008)
19. C. Moore, R.J. Blaikie, M.D. Arnold, Mater. Res. Soc. Symp. Proc. **1182** (2009)
20. P.K. Aravind, A. Nitzan, H. Metiu, Surf. Sci. **110**, 189 (1981)
21. E. Hao, G.C. Schatz, J. Chem. Phys. **120**, 357 (2004)
22. R.M. Bakker, A. Boltasseva, Z. Liu, R.H. Pedersen, S. Gresillon, A.V. Kildishev, V.P. Drachev, V.M. Shalaev, Opt. Express **15**, 13682 (2007)
23. V.M. Shalaev, M.I. Stockman, Sov. Phys. JETP **65**, 287 (1987)
24. V.A. Markel, L.S. Muratov, M.I. Stockman, T.F. George, Phys. Rev. B **43**, 8183 (1991)
25. V.M. Shalaev, Phys. Rep. **272**, 61 (1996)
26. V.A. Podolskiy, A.K. Sarychev, E.E. Narimanov, V.M. Shalaev, J. Opt. A, Pure Appl. Opt. **7**, S32 (2005)
27. U.K. Chettiar, A.V. Kildishev, T.A. Klar, V.M. Shalaev, Opt. Express **14**, 7872 (2008)
28. P. Muhlschlegel, H.J. Eisler, O.J.F. Martin, B. Hecht, D.W. Pohl, Science **308**, 1607 (2005)
29. W. Rechberger, A. Hohenau, A. Leitner, J.R. Krenn, B. Lamprecht, F.R. Aussenegg, Opt. Commun. **220**, 137 (2003)
30. J.N. Farahani, D.W. Pohl, H.-J. Eisler, B. Hecht, Phys. Rev. Lett. **95**, 017402 (2005)
31. Z. Liu, A. Boltasseva, R.H. Pedersen, R. Bakker, A.V. Kildishev, V.P. Drachev, V.M. Shalaev, Metamaterials **2**, 45 (2008)
32. Z. Liu, M.D. Thoreson, A.V. Kildishev, V.M. Shalaev, Appl. Phys. Lett. **95**, 033114 (2009)
33. K. Kneipp, M. Moskovits, H. Kneipp, *Surface-Enhanced Raman Scattering* (Springer, Berlin, 2006)
34. R.M. Bakker, V.P. Drachev, Z. Liu, H.-K. Yuan, R.H. Pedersen, A. Boltasseva, J. Chen, J. Irudayaraj, A.V. Kildishev, V.M. Shalaev, New J. Phys. **10**, 125022 (2008)
35. W.R. Tinga, W.A.G. Voss, D.F. Blossey, J. Appl. Phys. **44**, 3897 (1973)
36. V.M. Shalaev, *Nonlinear Optics of Random Media: Fractal Composites and Metal–Dielectric Films* (Springer, Berlin, 2000)
37. J. Sancho-Parramon, S. Bosch, A. Abdolvand, A. Podlipensky, G. Seifert, H. Graener, Proc. SPIE **5963**, 596320 (2005)
38. S. Novak, R. Hrach, Vacuum **84**, 174 (2010)
39. D.A.G. Bruggeman, Ann. Phys. (Leipzig) **24**, 636 (1935)
40. H. Liu, K.J. Webb, Opt. Lett. **33**, 2568 (2008)
41. W. Chen, M.D. Thoreson, S. Ishii, A.V. Kildishev, V.M. Shalaev, Opt. Express **18**, 5124 (2010)